

CHEMICAL EVOLUTION OF THE CIRCUMSTELLAR ENVELOPES OF CARBON-RICH POST-AGB OBJECTS

F. HERPIN^{1,2}, J.R. GOICOECHEA¹, J.R. PARDO^{1,3}, J. CERNICHARO^{1,3}¹Instituto de Estructura de la Materia, Departamento de Física Molecular, CSIC, Serrano 121, E-28006 Madrid, Spain

ABSTRACT

We have observed with the 30-m IRAM telescope, the CSO telescope and the ISO⁴ satellite (*Infrared Space Observatory*) the rotational lines of CO at millimeter, submillimeter and far infrared wavelengths in the direction of C-rich stellar objects at different stages of evolution : CRL 2688 (a very young Proto-Planetary Nebula), CRL 618 (a Proto-Planetary Nebula), and NGC 7027 (a young Planetary Nebula). Several changes in the longwave emission of CO and other molecules are discussed here in relation with the degree of evolution of the objects. In the early stages, represented by CRL 2688, the longwave emission is dominated by CO lines. In the intermediate stage, CRL 618, very fast outflows are present which, together with the strong UV field from the central star, dissociate CO. The released atomic oxygen is seen via its atomic lines, and allows the formation of new O-bearing species, such as H₂O and OH. The abundance of HNC is enhanced with respect to HCN as a result of the chemical processes occurring in the photo-dissociation region (PDR). At this stage, CO lines and [OI] lines are the dominant coolants, while the cooling effect of [CII] is rising. At the Planetary Nebula stage, NGC 7027, large parts of the *old* CO AGB material have been reprocessed. The spectrum is then dominated by atomic and ionic lines. New species such as CH⁺ appear. Water has probably been reprocessed in OH.

Subject headings: infrared: stars — line: identifications — planetary nebulae: individual (CRL 2688, CRL618, NGC7027) — stars: abundances — stars: carbon — stars: evolution

1. INTRODUCTION

Solar type stars remain in the asymptotic giant branch (AGB) for about $\sim 10^6 - 10^7$ years, losing mass through stellar winds ($\dot{M} \sim 10^{-4} - 10^{-7} M_{\odot}/\text{yr}$, ejection velocity $\sim 5 - 25 \text{ km s}^{-1}$, see, e.g., Loup et al. 1993). During this phase the ejected material progressively forms an expanding circumstellar envelope (CSE). Molecular species are easily formed in the innermost regions of the CSE. Some of these molecules aggregate onto dust grains which under the action of radiation pressure accelerate and push the remaining gas producing an expanding dusty molecular envelope. UV photons from the interstellar radiation field dissociate gas-phase molecules in the external layers of the envelopes allowing new chemical reactions and the production of new molecular species. These chemical changes have been very well studied through observations and models in the case of IRC+10216, the prototypical AGB carbon-rich star (Glassgold 1996; Cernicharo, Guélin & Kahane 2000 and references therein). Additional changes in the composition of the CSE do occur when the central object starts its evolution towards the white dwarf stage. A large UV field arises from the central (much hotter) star and at the same time, high velocity winds appear and interact with the AGB remnant (Cernicharo et al. 1989; Kwok 2000). Objects in this phase are called proto-planetary nebulae (hereafter *PPNe*). During this period (1000–2000 years; Bujarrabal et al. 2001), the almost spherical symmetry typical of the AGB stage disap-

pears and is replaced by a complicated geometrical structure (most PPNe are elliptical, bipolar or quadrupolar, Zuckerman & Aller 1986; Frank et al. 1993). The chemical composition is also strongly affected by these processes: O-bearing molecules can be formed in C-rich objects (Herpin & Cernicharo 2000), and complex organic molecules, which are not observed in IRC+10216, are efficiently produced (Cernicharo et al. 2001 a&b).

In order to better understand this evolution, we present in this paper a comparative study of the millimeter, submillimeter and far-IR CO line emission from 3 objects representing different stages of this fast transition: CRL 2688, a very young PPN, CRL 618, a PPN, and NGC 7027, a young planetary nebula (PN). The different excitation conditions of the observed CO lines allow to probe different layers in the CSEs. In particular, we study the CSE remnant wind and the higher velocity winds. The CSE component is the "normal" AGB wind, and the wind component refers to a higher velocity wind which is probably not present during the AGB phase and which contributes to changing the morphology from spherical to bi-polar or other non-spherical geometries. The observations are presented in section 2. The representativity of each selected source is discussed in section 3. Section 4 is devoted to the analysis of the spectra of IRC+10216 as a reference of the AGB phase. In section 5 we discuss the wind structure of the young PPN CRL 2688. Section 6 is devoted to CRL 618 and section 7 to the analysis of NGC 7027 observations. An overall comparative discussion of the four

²Present address: Observatoire de Bordeaux, B.P. 89, F-33270 Floirac, France, herpin@observ.u-bordeaux.fr

³Also visiting scientist at Division of Physics, Mathematics and Astronomy, California Institute of Technology, MS 320-47, Pasadena, CA, 91125, USA

⁴Based on observations with ISO, an ESA project with instruments funded by ESA Member States (especially the PI countries: France, Germany, the Netherlands and the United Kingdom) and with participation of ISAS and NASA.

objects is then presented in section 8.

2. OBSERVATIONS AND DATA ANALYSIS

The IRAM-30m observations of the CO 1–0 and 2–1 lines were performed in September 2000 using four SIS receivers with high (>0.90) image sideband rejection. The pointing and focus were checked using either Saturn or Jupiter, using the continuum emission of the sources and was found to be accurate to within $2''$. The typical system temperatures during these observations were 250 K (CO 1–0) and 400 K (CO 2–1). The observations used the wobbler system which provides very flat baselines. The spectrometers were a filterbank (at 115 GHz) and an autocorrelator (at 230 GHz) set to cover a band of 512 MHz with frequency resolutions of 1 and 1.25 MHz respectively (velocity resolutions of 2.60 and 1.63 km s^{-1} respectively).

The CO 3–2, 4–3, 6–5 and 7–6 observations were performed with the 10.4 m telescope of the Caltech Submillimeter Observatory at the summit of Mauna Kea (Hawaii) in September and October 2000 using three different receivers based on helium-cooled SIS mixers operating in double-sideband mode (DSB). The typical system temperatures during these observations were 750 K (CO 3–2) and 5000–6000 K (CO 4–3, 6–5 and 7–6). For further details about the receivers see Kooi et al. (2000) and references therein. The backends were two different acousto-optic spectrometers. One of them covers a bandwidth of 500 MHz with 1024 channels, and the other one covers 1.5 GHz with 2048 channels thus providing respectively the following velocity resolutions (in km s^{-1}): $146.38/\nu$ and $219.57/\nu$, with ν in GHz. The instantaneous band of the receivers, however, is ~ 0.9 GHz, thus limiting the validity of the data from the 1.5 GHz AOS to that range.

Since some of the CSO observations were performed shortly after a new 790–920 GHz receiver was installed for the first time at the telescope, its pointing and focus were carefully determined during previous runs earlier in the year. Then, the pointing of this and the other receivers was checked during our observations using Jupiter and Saturn first and then the own CO emission of each object. Taking into account that this emission is somewhat extended, the pointing is considered accurate to within $4''$ (CO 3–2, 4–3 lines) and $2''$ (CO 6–5 and 7–6 lines). The observations were also performed by wobbling the secondary reflector by $60''$. Proper corrections were finally applied to the data to compensate for the use of only one load (ambient temperature) in the chopper-wheel standard calibration of the CSO that relies upon the Penzias-Burrus (1973) approximation.

For the comparative discussion that we make further in this paper, fits of the CO mm/submm observations (shown in Fig. 1) of the three objects have been performed to derive the flow velocity of the different components and the integrated intensity ratio R_I between the emission of the CSE remnant and that of the wind for each transition. As angular resolution changes when observing at different frequencies and using different telescopes, the relative contribution to the bulk of the detected emission from the CSE remnant (extended) and the high velocity winds (unresolved) will be different. Hence, R_I outlines the wind

excitation of the different flows across the envelope (cf. Tables 1,2 and 3).

The ISO LWS Fabry-Perot data ($\lambda/\Delta\lambda \sim 9500$) of CRL 2688 were obtained during orbits 366 and 369. The integration times are 3400 and 5800 sec. The spectral resolution is 0.015 μm . The LWS grating mode (43–196.7 μm , $\lambda/\Delta\lambda \sim 200$) has a spectral resolution of 0.29 μm for the 43–93 μm range and 0.6 μm for the 80–196 μm range. LWS01 grating spectra for CRL 2688 and CRL618 were taken during orbits 21 and 688 respectively (total on-source times of 1218 sec and 5360 sec, respectively). The J=18–17 line of HCN was observed towards CRL 2688 during orbit 154 with the LWS grating mode and an integration time of 914 sec (see Fig. 4). Finally, the LWS grating spectra of NGC7027 taken by ISO during orbits 21, 342, 349, 356, 363, 377, 537, 552, 559, 566, 579, 587, 594, 601, 706, 713, 720, 727, 734, 741, 755, 762, 769, 776 and 783 were averaged. The total on-source time was 53409 sec. All data were processed following pipeline number 9 and treated with ISAP³ to remove glitches and fringes.

3. REPRESENTATIVITY OF THE SOURCE SAMPLE

In the next sections we try to identify and discuss the changes that occur through the transition of a C-rich AGB star to the PN stage. The aim of this work is to trace the evolution of the circumstellar chemistry in the late-AGB and post-AGB phases. This study is based on the analysis of the spectral differences observed in 4 objects: IRC+10216, CRL 2688, CRL 618 and NGC 7027. We thus have to rely upon the assumption that IRC+10216 will evolve into an object similar to the Egg Nebula, and then to an object similar to CRL 618 which will finally evolve to a planetary nebula that looks like NGC 7027. The ideal, but unfeasible approach, would be to observe a single object evolving through the post-AGB phase. In addition, our sample objects should be “typical” in the sense that each one should represent the averaged characteristics that the bulk of objects in the same stage of evolution.

However, CRL 2688, CRL 618 and NGC 7027 seem to be quite unusual objects in some properties, extreme cases among all carbon-rich AGB and post-AGB objects. All are very bright in molecular lines, but while IRC+10216 is a relatively close source (110–150 pc, Groenewegen et al. 1998, Crosas & Menten 1997), the other three objects are 5–10 times further away (Acker et al. 1992, Bujarrabal et al. 1994, Sahai et al. 1998). This may twist the comparison between IRC+10216 and the other sources, as distance influences line fluxes and profiles.

Recent works estimate a $\leq 2 M_{\odot}$ progenitor mass for IRC+10216 and place its core mass to 0.6 M_{\odot} (Kahane et al. 2000). Theoretical calculations suggest a progenitor main sequence mass of $\sim 3 M_{\odot}$ for both CRL 2688 and CRL 618 (Speck, Meixner and Knapp 2000), and 3–4 M_{\odot} for NGC 7027 (Sahai et al. 2001). IRC+10216 therefore, seems likely to evolve to the PN phase rather more slowly than the others, and this may affect the chemistry of the envelope. Anyway, several parallelisms exist between these objects: dense, optically thick dusty circumstellar

³The ISO Spectral Analysis Package (ISAP) is a joint development by the LWS and SWS Instrument Teams and Data Centers. Contributing institutes are CESR, IAS, IPAC, MPE, RAL and SRON.

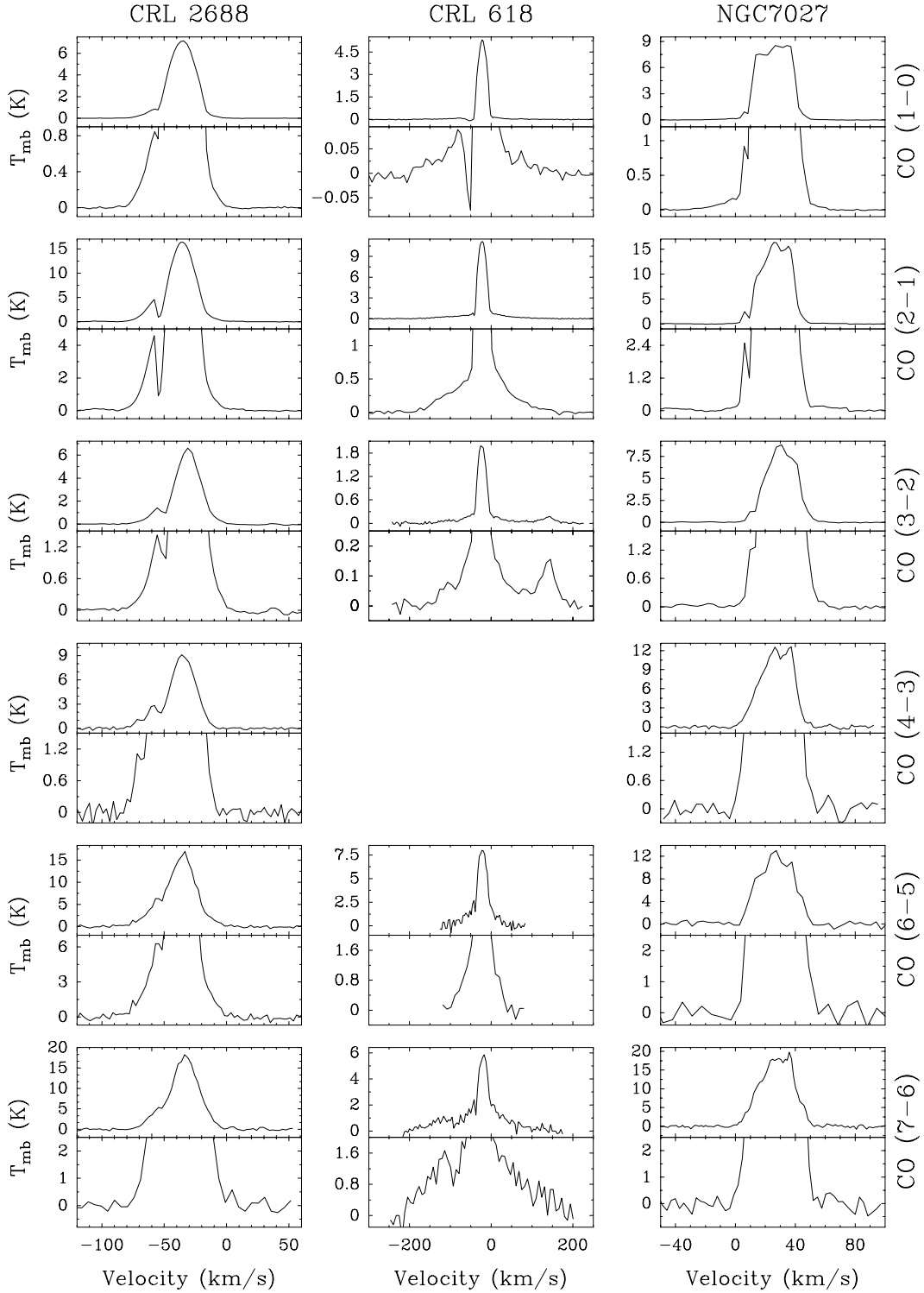


Fig. 1.— Spectra for the ^{12}CO $J=1-0$, $2-1$, $3-2$, $4-3$, $6-5$ and $7-6$ transitions for CRL 2688, CRL 618 (no $J=4-3$ observation) and NGC 7027. The main beam temperatures are in K and the velocity in km s^{-1} . Baselines were applied. The $1-0$ and $2-1$ lines are IRAM 30m observations; the others were made with the CSO; lines are smoothed. For each line, the upper part of the caption shows the whole profile, and the lower part shows the high velocity emission with an expanded vertical scale. Note that the emission present on the red part (at 141 km s^{-1}) of the CO ($3-2$) emission from CRL 618 is the HC_3N ($J=38-37$) line emission (at 345.609 GHz). The conversion factors Jy/K are respectively 4.3, 4.2 and 40 for the $1-0$, $2-1$ observations and rest of observations.

envelopes and shell-like density enhancements observed as incomplete arcs (Men'shchikov et al. 2001, Maun & Huggins 1999). These circumstellar concentric arcs, extremely pronounced in IRC+10216, are also detected in NGC 7027 (see Kwok, Su & Stoesz 2001). More generally, it has been proposed that further evolution of CRL 2688 will lead to morphologies similar to that observed in NGC 7027 (specially the ionized nebula and H₂ region; Cox et al. 1997).

The Egg Nebula is quite anomalous compared to more usual carbon-rich post-AGB objects. Its infrared spectrum is very different from that of any other carbon-rich post-AGB object, since it appears to be optically thick even at 30 μm (Omont et al. 1995). More common are the most extreme dusty carbon-stars such as the small group of sources discussed by Volk et al. (2000).

CRL 618 is quite similar to CRL 2688 in that both have massive molecular envelopes and central bipolar outflows (Meixner, Fong & Sutton 2001). However, CRL 618 shows an unusual rich circumstellar chemistry that could be related to its advanced stage of evolution (Herpin & Cernicharo 2000).

NGC 7027 is quite unusual among planetary nebulae in that it has a relatively massive circumstellar envelope beyond the ionized region. Its PDR is one of the densest and warmest in the PN sample studied by Liu et al. (2001). In fact, the ionized region is known to be relatively low in mass (≤ 0.2 solar masses, smaller than the typical values of 0.3-0.5 M_{\odot} of the ionized region of PN) while the surrounding mostly molecular gas totals 2-4 solar masses.

In conclusion, the objects selected here are rather peculiar in some properties that may influence their post-AGB evolution. However, a comparative study of their molecular envelopes could be useful to identify the distinct chemistries induced by the general physical changes produced by the different degrees of evolution, and this is the aim of this paper.

4. IRC+10216 : THE PROTOTYPICAL AGB CARBON-RICH OBJECT

To introduce this study, it is useful to present the main features of a typical object at the end of the AGB stage. IRC+10216 is the brightest AGB carbon rich star. Its estimated distance is 110–150 pc (Groenewegen 1997, Crosas & Menten 1997). It is believed to be in the final stage of red giant evolution and exhibits a bipolar reflection nebula (Skinner, Meixner & Bobrowsky 1998). The temperature of the central object is 2000 K, and the expansion velocity of the CSE is 14.5 km s^{-1} (Skinner, Meixner & Bobrowsky 1998; Cernicharo et al. 2000). IRC+10216 has an extended CSE where more than 50 molecular species have been detected (see line surveys by Cernicharo et al. 1996, Cernicharo et al. 2000). This object has a rich carbon chemistry and many of the species detected in its molecular envelope are carbon chain radicals which are formed in the external layers of the CSE (Cernicharo et al. 1996; Cernicharo et al. 2000). The innermost regions of the envelope are dominated by a chemistry at thermodynamical equilibrium (Tsuji 1973), where CO, HCN, C₂H₂, SiO are formed. As shown by Cernicharo et al. (1996), the far-IR spectrum consists of strong dust emission and several molecular emission lines from ¹²CO (J=14–13 to J=39–38), ¹³CO ($[^{12}\text{CO}/^{13}\text{CO}] \sim 45$), HCN (J=18–17

to J=48–47), H¹³CN and vibrationally excited HCN. The HCN lines have intensities similar to those of CO, and $[\text{HCN}/\text{CO}] = 1/10$, proving that HCN is the main coolant in the innermost region of the CSE. Only one ion, HCO⁺, has been detected (Lucas & Guélin 1999) and there is no [CII] line emission. The mid- and near-infrared spectra are dominated by the ro-vibrational lines of C₂H₂ and HCN (Cernicharo et al., 1999). The most abundant molecules through the CSE are CO, HCN and C₂H₂ (Fuente, Cernicharo & Omont 1998, Cernicharo et al. 2000).

The molecular observations of this object are well explained by a photochemical model (Glassgold 1996) considering that, due to the low effective temperature of the central star, the only UV photons available in the outer CSE come from the interstellar radiation field.

5. A YOUNG PPN: CRL 2688

CRL 2688 (the *Egg Nebula*) is a very young PPN (it has left the AGB phase probably only about 100 years ago) with an effective temperature around 6600 K (spectral type F5, Justtanont et al. 1997) and luminosity close to $1.8 \cdot 10^4 L_{\odot}$ (Jura & Kroto 1990). The non-detection of [OI] and [CII] (Cox et al. 1996) indicates that radiation from the central star has not yet formed a PDR. The molecular gas is in expanding fragmented shell structures, and shocks are thought to heat it (Cox et al. 1996). The AGB CSE expansion velocity is 20 km s^{-1} . CO emission has been seen as far as 42'' from the central object. The weaker ¹³CO emission extends over 20'' (Yamamura et al. 1996). Sahai et al. (1998) detected a moderate velocity wind (hereafter MVW) of 40 km s^{-1} with an angular extension of 10''. High velocity gas emerging in two different directions from the central star has been detected by Cox et al. (2000) in the CO J=2–1 emission line. The size of the emitting region is 4'' with extensions in both the north-south and east-west directions. Cox et al. (2000) have shown that this high velocity gas is closely related to the H₂ emission at 2 μm .

5.1. Low-excitation CO lines

The profiles of all low excitation CO lines (see Fig.1) are characteristic of optically thick emission. However, while the J=1–0, 2–1, and 3–2 lines probably trace the extended AGB remnant envelope of CRL 2688, higher J transitions are more sensitive to hotter gas from the inner layers of the envelope and hence of lower spatial extent. As J increases, the line opacities in the AGB CSE decrease and the emerging profiles change accordingly.

From the CO observations of CRL 2688 and the line parameters given in Table 1 we can distinguish two main outflows. The main one, the AGB CSE remnant, is centered at -35.4 km s^{-1} and covers around 20 km s^{-1} (in good agreement with Young et al. 1992). The second outflow has a moderate velocity extent, $\simeq 50 \text{ km s}^{-1}$, and is centered at -60 km s^{-1} . The intensity of the red wing of this MVW is weaker than its blue counterpart in the CO lines. We believe that this behavior is produced by AGB CSE remnant absorption of the MVW red wing.

An absorption dip is detected in the blue part of the mm and submm CO lines at $\simeq -55 \text{ km s}^{-1}$, just at the

Fabry–Perot CO lines in CRL2688

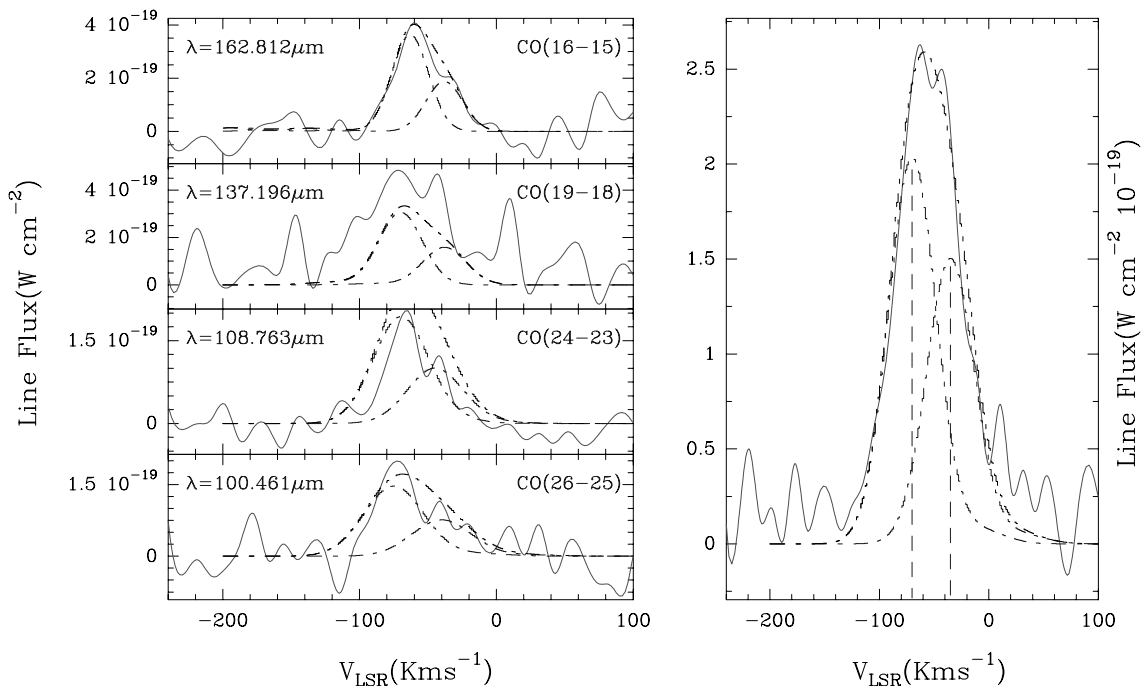


Fig. 2.— LWS/FP observations of ^{12}CO lines in CRL 2688 (left panel) and average spectra of all observed lines (right panel). The intensity scale corresponds to the continuum normalized flux rescaled to the values obtained with the LWS gratings for the same lines. The wavelength of each transition is indicated at the top left corner of each panel. The right panel shows the average spectra of the CO lines. Dashed lines show the fit produced by our LVG model as described in the text (with a center velocity precision of $\pm 15 \text{ km s}^{-1}$).

terminal velocity of the AGB CSE. It suggests that the low-velocity wind absorbs radiation from the inner and faster wind. Young et al. (1992) found that this absorption has a velocity width of $\approx 1 \text{ km s}^{-1}$ in the low-J lines. We found the same value for the J=6–5 and 7–6 CO lines. This would suggest that the microturbulence through the AGB CSE is nearly constant and equal to 1 km s^{-1} .

The ratio R_I goes from 0.08 (J=1–0) to 0.24 (J=7–6), stressing the importance of the MVW emission in the intermediate-J CO lines. The dilution of the MVW emitting region in the telescope beam will change with J. In addition, line opacities for the AGB CSE remnant and the MVW will also change differently with J. Hence, above a given rotational transition, the emission from the AGB CSE remnant will be weaker than that from the MVW. Observations of high excitation lines are thus needed in order to follow up the CO emission from the inner envelope.

5.2. Far-IR emission

Far-IR observations reveal the inner and hotter regions of the CSE where important chemical and physical processes are changing the structure of the AGB CSE. Rotational lines of ^{12}CO (J=14–13 to 26–25) are clearly detected while the emission from ^{13}CO is very weak. HCN is clearly detected in the AOT LWS02 grating spectrum of its J=18–17 transition (see Fig. 4, line detected with

$S/N \sim 4$; all the sub-peaks are smoothed noise). Note that some CO lines present broad wings at the grating resolution (see J=19–18, J=20–19, J=21–20) that are probably instrumental artefacts resulting from the defringing of the LWS data.

Several high-J CO (from J=16–15 to 26–25) lines were observed in Fabry-Perot mode with the LWS (see Fig. 2 for the J=16–15, J=19–18, J=24–23 and J=26–25 lines). The fluxes were divided by the continuum and rescaled to the values obtained for the same lines with the LWS grating. To derive more valuable information about kinematics and because the excitation and opacity is rather similar in all these lines, we computed an average spectrum (better S/N ratio) of all the individual lines (see right panel in Fig. 2). Study of this average CO LWS/FP spectrum reveals a much broader line than what we could expect from the AGB CSE remnant and centered at -65 km s^{-1} . It could prompt that all the emission is coming from the MVW. In order to estimate the CO emission at high-J from the AGB CSE remnant and from the MVW, we have fitted two gaussians to the average spectrum of Figure 2. We obtain velocities of $-70 \pm 10 \text{ km s}^{-1}$ and $-35 \pm 10 \text{ km s}^{-1}$ (see on the same figure the modelled emission from our *Large Velocity Gradient* (LVG) calculations -discussed below). These velocities agree, within the FP absolute wavelength calibration, with the MVW and AGB CSE velocities respectively. Obviously, higher spectral resolution observations are required to confirm both components (i.e.,

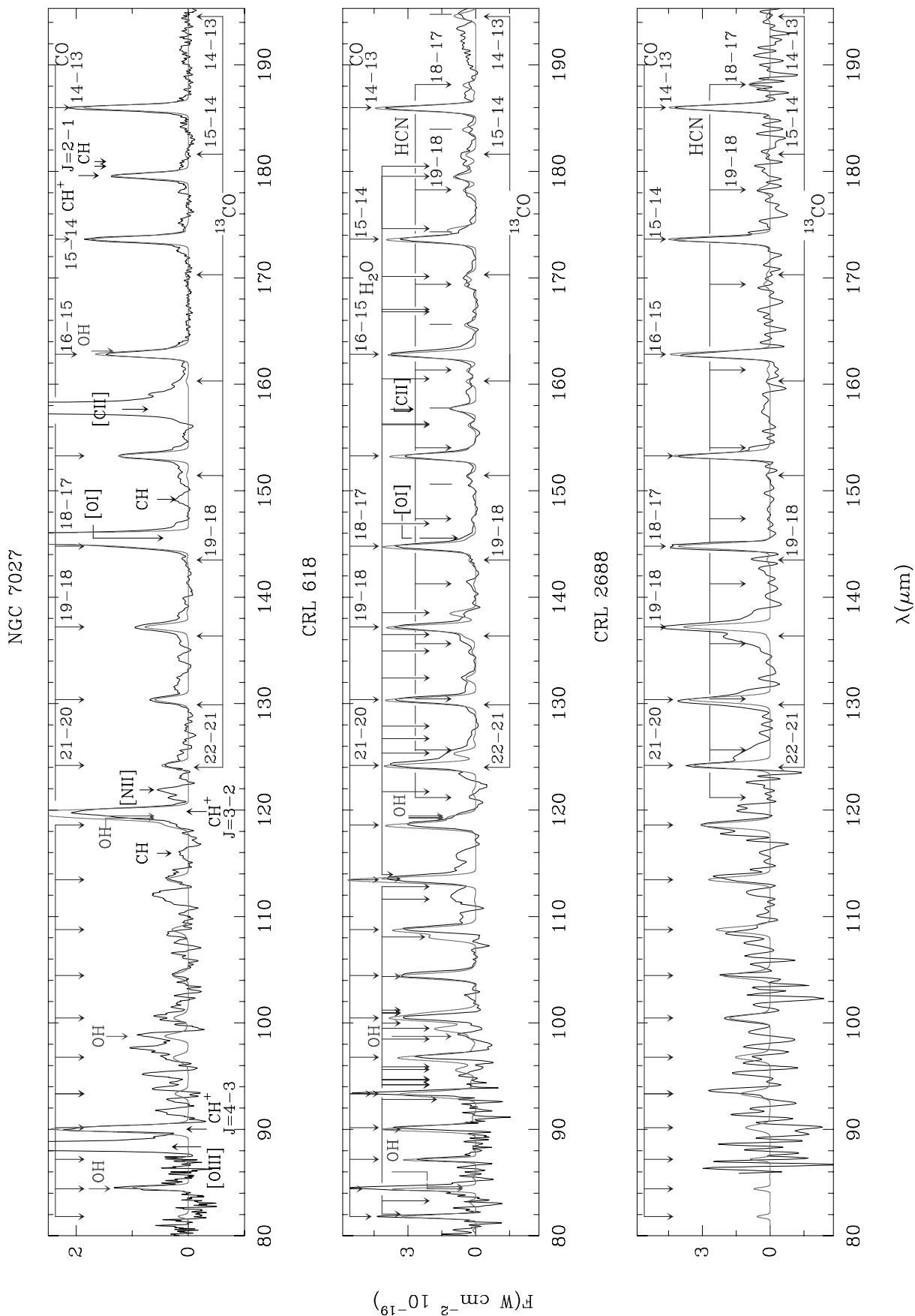


Fig. 3.— Continuum subtracted LWS spectra of CRL 2688 (bottom caption), CRL 618 (middle caption) and NGC 7027 (top caption). The result of our models is shown by the continuous grey line. The lines of ^{12}CO , ^{13}CO , HCN, H_2O , CH^+ and OH are indicated by arrows while those of HNC in CRL 618 are indicated by vertical lines (from $J=22-21$ at $150.627 \mu\text{m}$ to $J=17-16$ at $194.759 \mu\text{m}$). The [CII] and [OIII] lines are not included in our models; the plots indicate gaussian fits to these features.

HERSCHEL observations with HIFI). In the following we assume that both components emit in the high-J lines of CO and we will try to derive the relative contribution of each one.

Obviously, the average spectrum does not directly provide information on the column density of CO. In order to derive this parameter we have fitted the CO J=16–15 emission observed with the FP (the line with the best S/N ratio) with the two velocity components derived from the average spectrum. We then extended the result to the other lines (Fig. 2, left panel). Globally, the lines are well fitted by our model, with column densities of 85% (feature at -70 km s^{-1}) and 45% (feature at -35 km s^{-1}) with respect to the values retrieved from fitting the grating spectrum.

The red counterpart of the emission at -70 km s^{-1} is not detected. Our lines suggest that one part of the emission (at -70 km s^{-1}) comes from a wind with an outflow velocity of about 35 km s^{-1} , probably the MVW of Sahai et al. (1998). As the -70 km s^{-1} emission comes from a region where large shocks occur (interaction with the AGB remnant envelope), and the column density is thought to be larger, this emission appears stronger.

The other component (at the stellar velocity) is consistent with the wind velocity derived from our CO mm and submm observations (see Table 1). The widths of the emissions in each CO line show that the velocity dispersion is probably important in the excitation region.

In order to model the observed emission we have used an LVG code which divides the emitting source into several components with different solid angles (defined by θ). For each component we have fitted the column density of the molecule under consideration, the H_2 volume density and the temperature. Hence, the molecular abundance will depend on the layer thickness which cannot be derived in this retrieval scheme. While these assumptions could be correct for the high velocity wings and the PDR (CRL 618, NGC 7027), the component corresponding to the AGB remnant is poorly approximated as the whole CSE is reduced to a layer with a given average column density, temperature and density. This AGB remnant has been modelled in detail by Bujarrabal & Alcolea (1991).

The same basic physical parameters have been applied to ^{13}CO and HCN and we then only varied the column densities (see parameters in Table 4). For all the objects, model components were selected according to previous observational and theoretical works and our millimeter and submillimeter observations. The particular temperatures, solid angles, etc. are also derived from these studies, even if in some cases we adapt the parameters to correctly fit the data. Of course, column densities for each layer are sensitive to the excitation temperature.

According to other authors and our study of the low-J CO line emission, the adopted geometry model and physical parameters of each component are :

(i) An inner region representing the fast wind from the star (Sahai et al. 1998) and modelled as a layer of $\theta = 0.3''$, expansion velocity of $100\text{--}200 \text{ km s}^{-1}$, temperature of 800 K, and a density of $5 \cdot 10^7 \text{ cm}^{-3}$. The ^{12}CO column density (N) is $2 \cdot 10^{18} \text{ cm}^{-2}$ and the ^{13}CO and HCN abundances relative to ^{12}CO are $< 1/25$ and $< 1/100$ respectively. This hot component is needed to fit correctly the

high-J CO lines, as the single 400 K component of Cox et al. (1996) does not seem to be sufficient in our view.

(ii) As this fast wind slows down when shocking with the outer parts of the envelope, we have considered intermediate layers of larger sizes. Parameters are from Cox et al. (1996, 2000): a layer of 500 K, $\theta = 2''$, 100 km s^{-1} expansion velocity, and density of $5 \cdot 10^7 \text{ cm}^{-3}$. The ^{12}CO column density has decreased to $7 \cdot 10^{17} \text{ cm}^{-2}$ and the HCN/CO abundance ratio is $< 1/30$. An additional component is required where the wind has slowed down to 60 km s^{-1} , with a temperature of 400 K, $\theta = 3''$, density of $5 \cdot 10^7 \text{ cm}^{-3}$ and $N(^{12}\text{CO}) = 5 \cdot 10^{17} \text{ cm}^{-2}$. ^{13}CO and HCN have the same relative abundance ratios than in the previous layer.

(iii) A moderate velocity wind region (Sahai et al. 1998) with $\theta = 15''$, temperature of 250 K, density of $5 \cdot 10^7 \text{ cm}^{-3}$, velocity of 40 km s^{-1} , and ^{12}CO column density of $4.5 \cdot 10^{16} \text{ cm}^{-2}$. The relative abundances for the other species are the same as for previous layers.

(iv) The AGB remnant CSE where low-excitation CO emission extends beyond $40''$ (Cox et al. 1996, Yamamura et al. 1996) and that we have modelled as a layer of $25''$ at 50 K, expansion velocity of 20 km s^{-1} , $N(^{12}\text{CO}) = 3.5 \cdot 10^{16} \text{ cm}^{-2}$.

The global fit is shown in Figure 3 and reproduces reasonably well the LWS-ISO grating observations of CRL 2688. We also applied the same model to the mm and submm CO lines. Components (iii) and (iv) mainly fit the low-J CO lines (millimeter and submillimeter lines). Observed and predicted intensities are in good agreement (see Table 7).

5.3. Changes since the previous stage

With respect to the previous AGB stage, represented by IRC+10216, we see that the molecules emitting in the far-IR are basically the same, but with different relative intensities. This is probably due to the fact that the innermost region of the AGB remnant envelope has been already pushed away in these initial stages of the evolution towards the PPN phase. Hence, all the ro-vibrational lines of HCN have disappeared, not necessarily due to a depletion of this molecule but to the lack of sufficiently high temperatures and densities. This fact, together with the lack of [OI] and [CII], makes CO the main coolant of the envelope. The observational evidence of winds faster than those in the previous stage indicates that the gas in the inner layers is now heated by shocks, where the high-J CO lines excitation is favored. The presence of polyynes, as shown by the ISO mid-IR spectrum of this object (Cernicharo et al., 2001a), indicates that the envelope has also started an important chemical evolution when compared to IRC+10216. The high velocity winds and the increasing UV field from the central object are at the origin of this new chemistry, and this will be enhanced in the next stage (CRL 618).

6. A PPN OBJECT: CRL 618

CRL 618 is one of the few clear examples of an AGB star in the transition phase to the Planetary Nebula stage. There is evidence that this object must be a ~ 200 years old PPN (Bujarrabal et al. 1988). It has a compact HII region created by a hot central star (30 000 K, spectral type B0, Justtanont et al. 1997). CRL 618 is seen as a

bipolar nebula at optical, radio and infrared wavelengths (Carsenty & Solf 1982, Bujarrabal et al. 1988, Cernicharo et al. 1989, Neri et al. 1992, and Hora et al. 1996). The expansion velocity of the outer envelope is around 20 km s^{-1} . CO observations by Cernicharo et al. (1989) evidenced the presence of a high-velocity outflow ($\sim 200 \text{ km s}^{-1}$). The UV photons from the central star and this high velocity wind perturb the circumstellar envelope (CSE), producing shocks and photodissociation regions which modify the physical and chemical conditions of the gas (Herpin & Cernicharo 2000; Cernicharo et al. 2001a&b).

The molecular content of CRL 618 (Cernicharo et al. 2002, in preparation) is characterized by a large abundance of cyanopolyynes, acetylenic chains, methane, methylpolyynes and benzene (Cernicharo et al. 2001a&b): this PPN is a very efficient organic chemistry factory. The detection of long carbon chains in both CRL 618 and CRL 2688 suggests that the input of a UV radiation field from the evolving central object or/and the action of high velocity winds on the slowly expanding AGB remnant modify the CSE chemistry allowing the formation of new and more complex molecules.

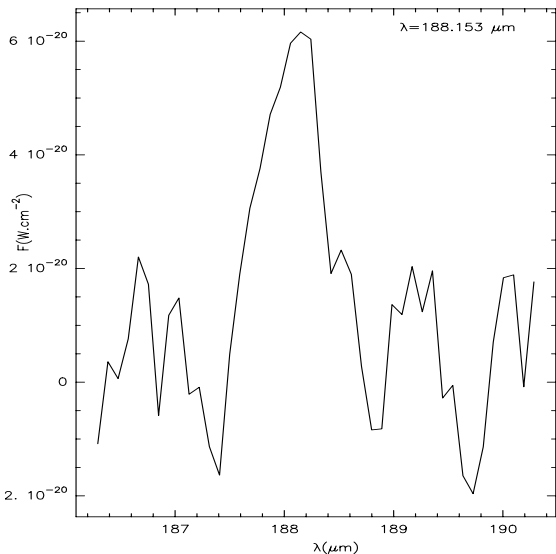


Fig. 4 –The HCN J=18–17 line emission detected by the LWS grating in CRL 2688 at a resolution of $0.6 \mu\text{m}$ ($S/\sim 4$).

6.1. Low-excitation CO lines

Two outflows can be seen in the CO line profiles of CRL 618 (see Table 2). The main outflow is centered at -22.0 km s^{-1} with an expansion velocity of roughly 20 km s^{-1} . The optically thick CO J=1–0 line clearly absorbs the continuum from -60 to -40 km s^{-1} coinciding with the main outflow terminal velocity. Other lines (higher transitions) show an absorption dip (self-absorption). In CRL 618, many molecular lines show P-Cygni profiles at 3 and 2 mm (Cernicharo et al. 2002). These lines, which correspond to very high energy ro-vibrational levels of HC_3N and HC_5N are formed in the PDR of the high density torus surrounding the central object.

The HVW (around 200 km s^{-1}), associated with a bi-conical outflow, is also observed in many other molecular transitions (see also Cernicharo et al. 1989, Cernicharo et al. 2002) but with a smaller velocity span. The CO wings

corresponding to this outflow have a smooth triangular shape and are present in all the millimeter and submillimeter lines. Their intensity increases with J, R_I going from 0.09 for J=1–0 to an estimated value of more than 2.6 in the J=7–6 line. Therefore, the emission in the high J lines (next paragraph) is basically dominated by this high velocity wind component.

6.2. Far-IR emission

The rotational lines of ^{12}CO (J=14–13 to J=41–40), ^{13}CO (J=14–13 to J=19–18), HCN, HNC, [OI] (at 63.170 and 145.526 μm) and [CII] ($^2p_{3/2} - ^2p_{1/2}$ transition at 157.74 μm) are observed in CRL 618 (see Fig. 3). Several lines of OH and H_2O are also detected. However, no H_2O emission has been detected at 183 GHz. As the 22, 183 and 321 GHz water maser lines are collisionally excited (radiative effects are small) in warm dense gas (Neufeld & Melnick 1990, 1991), this non-detection may indicate that water is not in the wind region, but rather in the torus.

The model used for analyzing the LWS observations of CRL 618 was presented in Herpin & Cernicharo (2000). Briefly, it consists of a central high density torus with its inner part being a Photo-Dissociated Region, an extended AGB remnant envelope and high velocity bipolar outflows. The physical parameters of the different layers are given in Table 5. The AGB remnant parameters are derived from Yamamura et al. (1994) and Hajian et al. (1996). The HVW characteristics are from Cernicharo et al. (1989), Neri et al. (1992) and Martin-Pintado et al. (1995). Justtanont et al. (2000) fit the ISO CO lines with a 700 K component ($n(\text{H}_2)=5 \cdot 10^7 \text{ cm}^{-3}$). Temperatures of the torus layers have been varied in order to get the best fit of the data. Our model, once applied to the low-excitation CO lines, disagrees with the observed J=3–2 to 7–6 intensities. This may be mainly explained by the completely non-spherical geometry of the source, and by the complex velocity field across the envelope. Moreover, as the CO molecules are reprocessed, excitation is more complex now and cannot be reproduced by our relatively simple model.

6.3. Changes since the previous stage

As in the previous very young PPN phase, shock chemistry plays an important role, as even faster outflows are detected. The now higher effective temperature of the central star induces a UV-based chemistry dominated by the photolysis of key molecules and the molecular content has started to be reprocessed. This fact is proved by the observed changes in molecular abundances (cf. HCN, HNC), the huge abundance of cyanopolyynes, the presence of polyynes and benzene (Cernicharo et al., 2001a&b) and of O-bearing molecules (Herpin and Cernicharo 2000). Ionic ([CII]) and atomic fine structure lines ([OI]) are also detected as a result of the photodissociation of CO. At this stage, the main cooling of the gas occurs via CO high-J, [CII] and [OI] lines.

7. A YOUNG PN OBJECT: NGC 7027

NGC 7027 is the most evolved object in this study. It is a very young PN, having left the AGB only 10^3 years

ago (Volk & Kwok 1997). The estimated temperature of the central star is around 200 000 K (Latter et al. 2000). The gas in the inner 10'' radius of the envelope has been completely ionized and a strong continuum emission arises from it. This region is revealed in the far-infrared by fine-structure lines (Liu et al. 1996). The PDR at the interface between the ionized and neutral regions is mainly traced by the pure rotational lines of CH⁺ (Cernicharo et al. 1997). The H₂ emission at this interface is found to be consistent with excitation by UV photons (Cox et al. 1997).

7.1. Low-excitation CO lines

All the CO lines are asymmetrical (see Fig.1), reflecting the complex kinematical structure of this PN. The main CO line emission is centered at $V_{LSR} \sim 27 - 30 \text{ km s}^{-1}$, with an expansion velocity of 15 km s^{-1} for the J=1-0, 2-1, 3-2 and 4-3 lines, and 20 km s^{-1} for the 6-5 and 7-6 lines (see Table 3). The higher velocity extent of the last two transitions probably indicates the presence of a faster wind at smaller radii (3'' - 5''). Jaminet et al. (1991) found $v_{exp} \sim 15 \text{ km s}^{-1}$ (with an angular extension of 5'' - 15'') for the 2-1 and 3-2 lines in agreement with our data for those transitions. They also have derived a velocity dispersion as high as 3 km s^{-1} at small radii (<5''), and more than 1 km s^{-1} in the outer parts (>5''). An absorption feature at $v_{LSR} \sim 10 \text{ km s}^{-1}$, due to self-absorption (Jaminet et al. 1991), is detected in the low-J lines (see Fig. 1).

Although the J=1-0 line of CO is certainly slightly contaminated by the 38 α recombination line of atomic hydrogen (shifted only by -8.3 km s^{-1} with respect to its center), the line profiles show also some emission at high velocity (mainly in the red part) that could be the signature of a faster outflow, with an estimated velocity extent of 45 km s^{-1} . This outflow component was not reported by Jaminet et al. (1991). They only found the extended outflow with $v_{exp} \sim 15 \text{ km s}^{-1}$ and a wind at a smaller radius with $v_{exp} \sim 23 \text{ km s}^{-1}$, which may be a flow driven by the pressure of the ionized region, and which is probably the place where the 6-5 and 7-6 lines are mainly excited (see v_{main} in Table 3). The flow at higher velocity ($\sim 47 \text{ km s}^{-1}$) may be the relic of a *High Velocity Wind* ejected during the PPN phase. Nevertheless, the importance of the wing emission is quite low as the ratio R_I is less than 0.1.

7.2. Far-IR emission

The J=14-13 to J=23-22 ¹²CO lines are detected in the LWS grating spectrum of NGC 7027 and some ¹³CO lines are also marginally detected. Despite its carbon rich chemistry, several lines of OH are clearly identified (Liu et al. 1997), while no H₂O emission is observed (Cernicharo et al. 1997). In addition to the molecular emission, strong atomic and ionic features typical of a PN spectrum are also seen. They include [OI], [CII], [NII], [NIII] and [OIII] lines. The pure rotational lines of CH⁺ discovered by Cernicharo et al. (1997) are prominent through the far-infrared spectrum. Features at 149.18 and 180.7 μm correspond to rotational lines of CH (see Liu et al. 1997). A new feature of this species at 115.9 μm is tentatively detected. However, no HCN or HNC emission is

seen, which supports the small HCN abundance ($9 \cdot 10^{-9}$) derived by Deguchi et al. (1990). The main cooling agents are fine-structure atomic and ionic lines.

To fit the far-infrared spectrum of NGC7027 we have considered 3 components (see Table 6): (i) the atomic region; (ii) a high density layer; (iii) the AGB remnant. Sizes of the different regions are derived from Yan et al. (1999) and Jaminet et al. (1991).

The atomic region (i) has been subdivided into two layers of 1000 K and 800 K and $\theta = 5''$ and $6''$ respectively (Cernicharo et al. 1997, Liu et al. 1996, Hasegawa, Volk & Kwok 2000). The density is $5 \cdot 10^7 \text{ cm}^{-3}$, and the expansion velocity 15 km s^{-1} . In the hottest layer, only [OI] and CH⁺ are present (for now we have not considered [CII] and [OIII], in the model although they are also present). In the external layer, we introduce ¹²CO, ¹³CO and OH. The considerable abundance of OH suggests that H₂O was probably present in the previous stage of evolution (see CRL 618), and, even if not detected, may be still present here, but with a low abundance. Thus we placed H₂O in region (i) with an upper limit of abundance relative to H₂ of $1.5 \cdot 10^{-7}$, according to the present data. This upper limit is 50% lower than the one obtained by Volk & Kwok (1997). The best fit to the data gives the following abundances (relative to ¹²CO) in this layer: $< 1/40$, $1/20$, $1/80$ and 875 for ¹³CO, OH, CH⁺ and [OI] respectively. Comparing with analyses performed by other authors we point out that the H₂ densities used in our model are higher than those of Liu et al. (1996), who took values between 10^5 and 10^6 cm^{-3} for the high-J CO lines coming from the hot region (1000-700 K). Also, the velocity of the expanding ionized region derived by Jaminet et al. (1991) is 17.6 km s^{-1} , while the estimated CO velocity wind by Sopka et al. (1989) is 17 km s^{-1} . Note that the two components of the atomic region produce similar lines, except that the hottest one only contains [OI] and CH⁺.

In the high density layer (ii) we consider a temperature of 270 K, $\theta = 9''$, expansion velocity of 15 km s^{-1} and a density of 10^6 cm^{-3} (Yan et al. 1999, Justtanont et al. 2000). Volk & Kwok (1997) applied for this layer very similar values ($n_{H_2} = 9 \cdot 10^5 \text{ cm}^{-3}$ and $T = 220 \text{ K}$). The fit results in a ¹²CO column density of $2.1 \cdot 10^{17} \text{ cm}^{-2}$ and [¹²CO / ¹³CO] ≤ 30 .

The AGB remnant region (iii) has an extension going from 10'' to 20'', the gas temperature decreases from 100 K to 50 K, and the density from $3 \cdot 10^5$ to 10^4 cm^{-3} (Hasegawa, Volk & Kwok 2000). The expansion velocity is 15 km s^{-1} (see Sect. 6.1 and Volk & Kwok 1997, Jaminet et al. 1991). The colder layer (50 K) is important here only to explain the low-J CO emission. The ¹²CO column density is 1.5 to $1.7 \cdot 10^{17} \text{ cm}^{-2}$ and the [¹²CO / ¹³CO] ratio is always < 30 . Note that CO emission extends over a region larger than 40'' (Masson et al. 1985).

Our lower limit of the ¹²C/¹³C ratio (30) is compatible with the value derived by Kahane et al. (1992) for this object (65) using much more sensitive millimeter observations of several carbon-bearing molecules. The whole CO column density derived by Thronson (1983) is larger than $2 \cdot 10^{17} \text{ cm}^{-2}$, in good agreement with our values.

The results of our model when applied to the low-excitation CO lines are satisfactory for J=1-0 to J=4-3, but the predicted intensities are too high for the J=6-5

and 7–6 lines. The reason might be the complex kinematical structure of this PN.

7.3. Changes since the previous stage

The main characteristic of this young PN compared with previous stages is the almost disappearance of fast molecular winds. The hot central object induces a strong UV field leading to a UV-dominated photochemistry in the envelope. As a consequence, molecular abundances have been strongly modified since the PPN phase. Water vapor and HCN have almost disappeared, while other species such as CH^+ have been efficiently formed. The cooling effect of CO lines is much weaker and now the gas is mainly cooling via ionic and atomic fine structure lines.

8. DISCUSSION

- It is assumed that CRL 2688 has just left the AGB phase: the central object is not yet sufficiently hot to produce a significant ionization or photodissociation of the gas. Hence, the far-IR molecular emission (^{12}CO , ^{13}CO , HCN) is well reproduced by our model. Nevertheless, the detection of the polyynes C_4H_2 and C_6H_2 in this object indicates that some chemical processing has already started, an important difference as respects to IRC+10216 where these species are not detected.

In addition to the low expanding AGB CSE remnant, this PPN exhibits an inner and faster outflow which runs into that AGB envelope. This is one of the main characteristics of an object beginning its transition to the PN stage. At this point, emission from the molecular gas is the main cooling process.

The ^{13}CO emission is not detectable at the low sensitivity of the LWS grating spectrum. For a ^{12}CO abundance of $6 \cdot 10^{-4}$ the upper limit of ^{13}CO abundance would be $< 2.2 \cdot 10^{-5}$. This value is half of what was found by Yamamura et al. 1996 ($4 \cdot 10^{-5} - 7.5 \cdot 10^{-5}$), but is similar to the ^{13}CO abundance found in an AGB star such as IRC+10216 ($1-3 \cdot 10^{-5}$, Cernicharo et al. 1996). However, Kahane et al. (1992) derived more accurate isotopic ratios, $3.7 \cdot 10^{-5}$ and $7.5 \cdot 10^{-5}$, respectively for IRC+10216 and CRL 2688, showing an increase by a factor of 2. For Jaminet et al. (1992), CNO nuclear processing in the star injects material into the stellar wind: in the slow wind, $[\text{}^{12}\text{CO}/\text{}^{13}\text{CO}] = 20$, while in the fast wind they find a ratio of 5. Because of these values, these authors placed CRL 2688 among the J-type carbon stars, which have a considerably lower $^{12}\text{CO}/^{13}\text{CO}$ ratio than carbon stars (40–80). However, we prefer to argue that CRL 2688 has just begun to evolve to the PN stage; the ^{12}CO material has just begun to be reprocessed, as proved by the apparent increase of the ^{13}CO abundance between IRC+10216 and CRL 2688.

The HCN/CO ratio in IRC+10216 is 0.1, much larger than in the high velocity winds of the post-AGB envelopes discussed here. According to our model, we find a lower HCN abundance (relative to ^{12}CO) in the fast wind ($\leq 6 \cdot 10^{-6}$) than in the slow wind ($\leq 2 \cdot 10^{-5}$, i.e., similar to IRC+10216). Sopka et al. (1989) found $3.3 \cdot 10^{-6}$ in the fast wind while Jaminet et al. (1992) found $7 \cdot 10^{-7}$.

HNC is not detected in this object. This molecule is mainly formed by ion-molecule reactions, and in this post-AGB envelope, physical conditions are therefore not very

suitable for a considerable HNC production. Moreover, Yamamura et al. (1996) and Sopka et al. (1989) derived $[\text{HCN}/\text{HNC}] \sim 21$ and 160 respectively. According to this fact, the HNC emission is largely under our detection limit.

- In CRL 618, Herpin & Cernicharo (2000) have shown that O-bearing species, H_2O and OH, are produced in the innermost region of the circumstellar envelope. Also Cernicharo et al. (2001 a&b) have detected in this object the poly-acetylenic chains C_4H_2 and C_6H_2 , methyl-polyynes, and benzene. The UV photons from the central star photodissociate most of the molecular species produced in the AGB phase and allow a chemistry dominated by standard ion-neutral reactions. O-bearing species are formed, and also abundances of C-rich molecules such as HCN and HNC are modified (see Table 7). At the high temperatures of the PDR, OH can be formed by endothermic reactions between O and H_2 , with O released by CO photodissociation, and then can produce H_2O through reactions with H_2 . H_2O and OH can also be produced from the dissociative recombination of H_3O^+ if this ion is abundant enough.

- NGC 7027 has a very hot central star. Because of the high UV flux ($10^4 \leq G_0 \leq 10^5$, Burton et al. 1990), there is a strong presence of atomic lines. UV photons from the central star produce a PDR and the gas cools mainly via fine-structure atomic lines. In the PDR, the total number of CO molecules is around 2% of that of ionized carbon, i.e. most of the CO molecules have been photodissociated (Liu et al. 1996). As the ionized region is not modeled in this work, our results concerning the atomic region have to be carefully taken: in the high electron density environment of NGC 7027, ionic fine-structure lines are strongly suppressed by collisional de-excitation (Liu et al. 1996, Keyes et al. 1990). Electron impact may be important in exciting the CH^+ lines and would lower the CH^+ abundance (Cernicharo et al. 1997). In the 1000 K layer, the formation of CH^+ may be achieved via $\text{C}^+ + \text{H}_2 \rightarrow \text{CH}^+ + \text{H}$ (activation energy of ~ 4000 K). The formation rate of CH^+ (Sternberg & Dalgarno 1995) could be high enough to produce column densities similar to those derived in this work. Due to the high temperatures, densities and UV radiation field in the PDR, the formation of CH^+ leads to the creation of CH_2^+ and CH_3^+ , whose dissociative recombination will form CH very efficiently at a temperature of 800 K (Sternberg & Dalgarno 1995); Liu et al. (1997) derived $[\text{CH}/\text{CH}^+] \sim 0.2$. The observed CH lines are excited by collisions with atomic and molecular hydrogen.

The presence of [OI] and CH^+ in the 1000 K layer of the atomic region, and the low abundance of CO in the 800 K layer, indicate that the CO molecules have been largely reprocessed there through UV photons. Note that the chemical model of Hasegawa, Volk & Kwok (2000) shows that the CO observed in these objects consists of new formed molecules. Nevertheless, the AGB circumstellar gas has not been totally reprocessed: the ionized and photodissociation regions still constitute a relatively small but significant fraction of the total mass of the circumstellar material around NGC 7027.

The study of CRL 618 showed that H_2O and OH can be efficiently produced. However, these O-bearing species are also quickly reprocessed. This is seen in the next stage, represented by NGC 7027. The equilibrium models (Mc-

Cabe, Connon, Smith & Clegg 1979) predict essentially no water in the carbon-rich conditions of the NGC 7027 envelope. Volk & Kwok (1997) argue that even under non-equilibrium chemical conditions, only a very small fraction of oxygen will be converted to water here. The non detection of H₂O and the detection of OH in NGC 7027 indicate that H₂O molecules formed in the previous stage may have been almost entirely reprocessed. In the NGC 7027 environment, the simplest explanation for the water vapor disappearance is its transformation into OH and H by UV photo-dissociation. This will explain the increase of OH abundance by a factor 60 since the previous PPN stage represented by CRL 618. Concerning HCN, probably most molecules have been photodissociated into H and CN (CN was detected by Bachiller et al. 1997 with a strong abundance, CN/HCN=9). Photo-dissociation of CO, HCN, and other carbon-bearing molecules contribute to the increase of carbon ions abundance.

9. CONCLUSION

The study of the selected 3 objects in rapid evolution from the AGB to the PN stage clearly shows the crucial importance that (i) the interaction between fast and slow winds; and (ii) the increase of UV flux as the central object evolves toward the white dwarf state have on the chemistry. The spectroscopic evidence of the increasing UV flux comes from the appearance of atomic and ionic lines in CRL 618, which later dominate the far-IR spectrum of NGC 7027. Atomic and ionic lines tend to appear (at ISO's sensitivity) when the central star is hotter than 10000 K (Fong et al. 2001; Castro-Carrizo et al. 2001). On the other hand, the spectroscopic signature showing that shocks become less important as the evolution goes on, comes from the wind velocity decrease seen in the CO profiles (this must be confirmed by further studies on more objects and only refers to the neutral gas). The strongest shocks occur just after leaving the AGB when the central

star is ejecting large amounts of material in a very fast wind (the case of CRL 2688). The AGB remnant envelope is being shocked by an inner, faster wind developed in the PPN stage (i.e., the 200 km s⁻¹ wind in CRL 618). Most of the ¹²CO, ¹³CO and HCN emission is produced in these shocks. The fast increase of the stellar temperature, will produce a new UV-dominated chemistry when $T_{eff} \geq 30000$ K. These new conditions (UV photons and shocks) will deeply modify the constitution of the inner parts of the envelope. Indeed, in CRL 618, O-bearing molecules (H₂O and OH, Herpin and Cernicharo 2000) and relatively complex organic molecules (Cernicharo et al., 2001a&b) appear. Furthermore, most of the CO and HCN will be entirely reprocessed in the PDR leading to strong HNC emission. At this point, CO and [OI] atomic lines are the dominant coolants.

As the star reaches the PN stage, the strong fast molecular winds have disappeared, and slow expanding layers constitute the PN envelope around a large and hot atomic region. Most of the *old* AGB material has been reprocessed. The spectrum is now dominated by atomic and ionic lines. New species such as CH⁺ and CH appear. There is only weak HCN emission, as the molecules may have been broken into H and CN. More interesting is the disappearance of H₂O, which has probably also been reprocessed, and is only a relatively abundant molecule in the intermediate C-rich PPN stage.

Acknowledgments We thank Spanish DGES, CICYT, and PNIE for funding support for this research under grants PB96-0883, ESP98-1351E and PANAYA2000-1784. JRG acknowledges UAM for a pre-doctoral fellowship. JRP also acknowledges further support for his research from NSF grants AST99-80846 (CSO operations) and ATM96-16766. We thank Dr. V. Bujarrabal for useful comments and suggestions. We thank the anonymous referee for his useful comments which result in an important improvement of this paper.

REFERENCES

- Acker, A. et al. 1992, Strasbourg-ESO catalog of galactic planetary nebulae, ESO, Garching
 Bachiller, R., Forveille, T., Huggins, P.J., Cox, P. 1997, A&A 324, 1123
 Bujarrabal, V., Gómez-González, J., Bachiller, R., Martín-Pintado, J. 1988, A&A 204, 242
 Bujarrabal, V., & Alcolea, J. 1991, A&A, 251, 536
 Bujarrabal, V., Fuente, A., Omont, A. 1994, A&A 285, 247
 Bujarrabal, V., Castro-Carrizo, A., Alcolea, J., & Sánchez-Contreras, C. 2001, A&A, 377, 868
 Burton, M.G., Hollenbach, D.J., Tielens, A.G.G.M. 1990, ApJ 365, 620
 Carsenty, U., Solf, J. 1982, A&A 106, 307
 Castro-Carrizo, A., Bujarrabal, V., Fong, D. et al. 2001, A&A 367, 674
 Cernicharo, J., Guélin, M., Martín-Pintado, J., Peñalver, J., Mauersberger, R. 1989, A&A 222, L1
 Cernicharo, J., Barlow, M.J., González-Alfonso, E., et al. 1996, A&A 315, L201
 Cernicharo, J., Liu, X.W., González-Alfonso, E., Cox, P., Barlow, M.J., Lim, T., Swinyard, B.M. 1997, ApJ 483, L65
 Cernicharo, J., Yamamura, I., González-Alfonso, E., et al. 1999, ApJ 526, L41
 Cernicharo, J., Guélin, M., Kahane, C. 2000, AASS 142, 181
 Cernicharo, J., Heras, A.M., Tielens, A.G.G.M., et al. 2001a, ApJ Letters 546, L123
 Cernicharo, J., Heras, A.M., Pardo, J.R., et al. 2001b, ApJ Letters 546, L127
 Cox, P., González-Alfonso, E., Barlow, M.J., et al. 1996, A&A 315, L265
 Cox, P., Maillard, J.P., Huggins, P.J., et al. 1997, A&A 321, 907
 Cox, P., Lucas, R., Huggins, P.J., Forveille, T., Bachiller, R., Guilleloteau, S., Maillard, J.P., Omont, A., 2000 A&A 353, L25
 Crosas, M., Menten, K.M., 1997 ApJ 483, 913
 Deguchi, S., Izumiura, H., Kaifu, N., Mao, X., Nguyen-Q-Rieu, Ukita, N., 1990 ApJ 351, 522
 Fong, D., Meixner, M., Castro-Carrizo, A., Bujarrabal, V., Latter, W.B., Tielens, A.G.G.M., Kelly, D.M., Sutton, E.C. 2001, A&A, 367, 652
 Frank, A., Balick, B., Icke, V., Mellema, G., 1993 ApJ 404, L25
 Fuente, A., Cernicharo, J., Omont, A., 1998 A&A 330, 232
 Glassgold, A.E. 1996, ARAA 34, 241
 Groenewegen, M.A.T. 1997, A&A 317, 503
 Groenewegen, M.A.T., van der Veen, W.E.C.J., Mattheus, H.E. 1998, A&A 338, 491
 Hajian, A. R., Phillips, J. A., Terzian, Y. 1996, ApJ 467, 341
 Hasegawa, T., Volk, K., Kwok, S. 2000, ApJ 532, 994
 Herpin, F., Cernicharo, J., 2000 ApJ 530, L129
 Hora, J.L., Deutsch, L.K., Hoffmann, W.F., Fazio, G.G. 1996, AJ 112, 2064
 Jaminet, P.A., Danchi, W.C., Sutton, E.C., et al. 1991, ApJ 380, 461
 Jaminet, P.A., Danchi, W.C., Sandell, G., Sutton, E.C. 1992, ApJ 400, 535
 Jura, M., Kroto, H. 1990, ApJ 351, 222
 Justanont, K., Tielens, A.G.G.M., Skinner, C.J., Haas, M.R. 1997, ApJ 476, 319
 Justanont, K., Barlow, M.J., Tielens, A.G.G.M., et al. 2000, A&A 360, 1117

- Kahane, C., Cernicharo, J., Gómez-González, J., Guélin, M. 1992, *A&A* 256, 235
- Kahane, C., Dufour, E., Busso, M. et al. 2000, *A&A* 357, 669
- Keyes, C.D., Aller, L.H., Feibelman, W.A. 1990, *PASP* 102, 59
- Kooi, J.W., Kawamura, J., Chen, J., et al. 2000, *Int. J. of Infrared and Millimeter Waves*, 21, 9
- Kwok, S. 2000, in *The origin and evolution of planetary nebulae*, Cambridge astrophysics series 31, Cambridge university press
- Kwok, S., Su, K.Y.L., Stoesz, J.A. 2001, in *Post-AGB objects as a phase of stellar evolution*, edited by R. Szczerba and S.K. Gorny, *Astrophys. and Space Science Library*, vol. 265
- Latter, W.B., Dayal, A., Bieging, J.H., et al. 2000, *ApJ* 539, 783
- Liu, X.W., Barlow, M.J., Nguyen-Q-Rieu, et al. 1996, *A&A* 315, L257
- Liu, X.W., Barlow, M.J., Dalgarno, A., et al. 1997, *MNRAS* 290, L71
- Liu, X.W. et al. 2001, *MNRAS* 323, 343
- Loup, C., Forveille, T., Omont, A., Paul, J.F. 1993, *AASS* 99, 291
- Lucas, R., Guélin, M. 1999, in *Asymptotic giant branch stars*, p.305, IAU symposium 191, published by the Astronomical Society of the Pacific
- McCabe, E.M., Connon Smith, R., Clegg, R.E.S. 1979, *Nature* 281, 263
- Martin-Pintado, J., Gaume, R. A., Johnston, K. J., Bachiller, R. 1995, *ApJ* 446, 687
- Masson, C.R., Cheung, K.W., Berge, G.L., et al. 1985, *ApJ* 292, 464
- Mauron, N., Huggins, P.J. 1999, *A&A* 349, 203
- Men'shchikov, A.B., Bolega, Y., Blöcker, T. et al. 2001, *A&A* 368, 497
- Meixner, M., Fong, D., Sutton, E.C., Welch, W.J. 2001, in *Post-AGB objects as a phase of stellar evolution*, edited by R. Szczerba and S.K. Gorny, *Astrophys. and Space Science Library*, vol. 265
- Neri, R., Garcia-Burillo, S., Guélin, M., Cernicharo, J., Guilloteau, S., Lucas, R. 1992, *A&A* 262, 544
- Neufeld, D., Melnick, G. 1990, *ApJ* 352 L9
- Omont, A., Moseley, S.H., Cox, P. 1995, *ApJ* 454, 819
- Penzias, A.A., Burrus, C.A. 1973, *ARA&A* 11, 51
- Sahai, R., Trauger, J.T., Watson, A.M., et al. 1998, *ApJ* 493, 301
- Salas, J.B., Pottasch, S.R., Beintama, D.A., Wesselius, P.R., 2001 *A&A* 367, 949
- Skinner, C.J., Meixner, M., Bobrowsky, M. 1998, *MNRAS* 300, L29
- Sopka, R.J., Olofsson, H., Johansson, L.E.B., Nguyen Q-Rieu, Zuckerman, B. 1989, *A&A* 210, 78
- Speck, A.K., Meixner, M., Knapp, G.R. 2000, *ApJ* 545, L145
- Sternberg, A., Dalgarno, A. 1995, *ApJS* 99, 565
- Thronson, H.A. 1983, *ApJ* 264, 599
- Tsuji, T. 1973, *A&A* 23, 411
- Volk, K., Kwok, S. 1997, *ApJ* 477, 722
- Volk, K., Xiong, G.-Z., Kwok, S. 2000, *ApJ* 454, 819
- Yamamura, I., Shibata, K.M., Kasuga, T., Deguchi, S. 1994, *ApJ* 427, 406
- Yamamura, I., Onaka, T., Kamijo, F., Deguchi, S., Ukita, N. 1996, *ApJ* 465, 926
- Yan, M., Federman, S.R., Dalgarno, A., Bjorkman, J.E. 1999, *ApJ* 515, 640
- Young, K., Serabyn, G., Phillips, T.G. et al. 1992, *ApJ* 385, 265
- Zuckerman, B., Aller, L.H. 1986, *ApJ* 301, 772

TABLE 1

Table of the parameters for the different flows in CRL 2688. The uncertainty on v_{main} and v_{wing} is 0.3 km s^{-1} . R_I is the wing and main integrated intensities ratio.

CO parameters	CRL 2688					
	1-0	2-1	3-2	4-3	6-5	7-6
v_{main} (km s^{-1})	19.3	20.0	23.9	24.1	23.4	23.3
v_{wing} (km s^{-1})	50.0	52.0	50.7	40.3	41.6	33.3
R_I	0.08	0.08	0.11	0.16	0.24	0.24
ΔR_I	(0.01)	(0.01)	(0.01)	(0.02)	(0.02)	(0.03)

TABLE 2

Table of the parameters for the different flows in CRL 618. The uncertainty on v_{main} and v_{wing} is 0.3 km s^{-1} . R_I is the wing and main integrated intensities ratio. For the 6-5 and 7-6 lines, the parameters v_{Wing} and R_i are lower limits due to the insufficient bandwidth available for these observations.

CO parameters	CRL 618				
	1-0	2-1	3-2	6-5	7-6
v_{main} (km s^{-1})	19.7	19.6	18.9	17.1	18.8
v_{wing} (km s^{-1})	202.5	204.5	178.5	>76.0	≥ 195.0
R_I	0.09	0.22	0.45	>0.72	≥ 2.6
ΔR_I	(0.01)	(0.02)	(0.03)	(0.05)	(0.3)

TABLE 3

Table of the parameters for the different flows in NGC 7027. The uncertainty on v_{main} and v_{wing} is 0.3 km s^{-1} . R_I is the wing and main integrated intensities ratio.

CO parameters	NGC 7027					
	1-0	2-1	3-2	4-3	6-5	7-6
v_{main} (km s^{-1})	14.6	14.3	16.0	18.3	20.0	20.0
v_{wing} (km s^{-1})	47.2	43.2	30.0	25.1	24.7	23.8
R_I	0.04	0.09	0.07	0.07	0.06	0.09
ΔR_I	(0.01)	(0.01)	(0.02)	(0.02)	(0.02)	(0.02)

TABLE 4

Table of the column densities (in cm^{-2}) obtained from our model for all molecules present in each region of CRL 2688 (θ defines the solid angle of each considered layer).

Molecules	^{12}CO	^{13}CO	HCN
FAST WIND FROM THE STAR (i)			
T=800 K, $\theta = 0.3''$, $v = 200 \text{ km s}^{-1}$, $n(\text{H}_2) = 5 \cdot 10^7 \text{ cm}^{-3}$	$2 \cdot 10^{18}$	$< 8 \cdot 10^{16}$	$< 2 \cdot 10^{16}$
T=500 K, $\theta = 2''$, $v = 100 \text{ km s}^{-1}$, $n(\text{H}_2) = 5 \cdot 10^7 \text{ cm}^{-3}$	$7 \cdot 10^{17}$	$< 2.8 \cdot 10^{16}$	$< 2.3 \cdot 10^{16}$
T=400 K, $\theta = 3''$, $v = 60 \text{ km s}^{-1}$, $n(\text{H}_2) = 5 \cdot 10^7 \text{ cm}^{-3}$	$5 \cdot 10^{17}$	$< 2 \cdot 10^{16}$	$< 1.7 \cdot 10^{16}$
MEDIUM WIND FROM THE STAR (ii)			
T=250 K, $\theta = 15''$, $v = 40 \text{ km s}^{-1}$, $n(\text{H}_2) = 5 \cdot 10^7 \text{ cm}^{-3}$	$4.5 \cdot 10^{16}$	$< 1.8 \cdot 10^{15}$	$< 1.5 \cdot 10^{15}$
AGB remnant (iii)			
T=50 K, $\theta = 25''$, $v = 20 \text{ km s}^{-1}$, $n(\text{H}_2) = 5 \cdot 10^5 \text{ cm}^{-3}$	$3.5 \cdot 10^{16}$	$< 1.4 \cdot 10^{15}$	$< 1.2 \cdot 10^{15}$

TABLE 5

Table of the column densities (in cm^{-2}) obtained from our model for all molecules present in each region of CRL 618 (θ defines the solid angle of each considered layer).

Molecules	^{12}CO	^{13}CO	HCN	HNC	<i>o</i> -H ₂ O	OH	[OI]
TORUS (including PDR)							
T=250 K, $\theta = 1.5''$	10^{19}	$5 \cdot 10^{17}$	10^{16}	10^{16}	$3 \cdot 10^{17}$	$8 \cdot 10^{15}$	
$v = 20 \text{ km s}^{-1}$, $n(\text{H}_2) = 5 \cdot 10^7 \text{ cm}^{-3}$							
T=800 K, $\theta = 1.1''$	$6 \cdot 10^{17}$	$3 \cdot 10^{16}$					
$v = 20 \text{ km s}^{-1}$, $n(\text{H}_2) = 5 \cdot 10^7 \text{ cm}^{-3}$							
T=1000 K, $\theta = 0.6''$	10^{19}	$5 \cdot 10^{17}$					$4.5 \cdot 10^{19}$
$v = 20 \text{ km s}^{-1}$, $n(\text{H}_2) = 7 \cdot 10^7 \text{ cm}^{-3}$							
HVW							
T=200 K, $\theta = 1.7''$	$5 \cdot 10^{18}$	$2.5 \cdot 10^{17}$	$3 \cdot 10^{17}$	$2 \cdot 10^{17}$			
$v = 50 \text{ km s}^{-1}$, $n(\text{H}_2) = 10^7 \text{ cm}^{-3}$							
T=1000 K, $\theta = 1.5''$	$2 \cdot 10^{16}$	$1 \cdot 10^{15}$	$2 \cdot 10^{15}$	10^{14}			
$v = 200 \text{ km s}^{-1}$, $n(\text{H}_2) = 10^7 \text{ cm}^{-3}$							
AGB remnant							
T=50 K, $\theta = 10''$	$7 \cdot 10^{17}$	$3.5 \cdot 10^{16}$	$7 \cdot 10^{16}$	$7 \cdot 10^{14}$			
$v = 20 \text{ km s}^{-1}$, $n(\text{H}_2) = 10^5 \text{ cm}^{-3}$							

TABLE 6

Table of the column densities (in cm^{-2}) obtained from our model for all molecules present in each region of NGC 7027 (θ defines the solid angle of each considered layer).

Molecules	^{12}CO	^{13}CO	<i>o</i> -H ₂ O	OH	[OI]	CH ⁺
ATOMIC REGION (i)						
T=1000 K, $\theta = 5''$					$2 \cdot 10^{19}$	$9 \cdot 10^{13}$
$v = 15 \text{ km s}^{-1}$, $n(\text{H}_2) = 5 \cdot 10^7 \text{ cm}^{-3}$						
T=800 K, $\theta = 6''$	$8 \cdot 10^{15}$	$2.7 \cdot 10^{14}$	$< 2.6 \cdot 10^{13}$	$4 \cdot 10^{14}$	$7 \cdot 10^{18}$	10^{14}
$v = 15 \text{ km s}^{-1}$, $n(\text{H}_2) = 5 \cdot 10^7 \text{ cm}^{-3}$						
HIGH DENSITY LAYER(ii)						
T=270 K, $\theta = 9''$	$2.1 \cdot 10^{17}$	$7 \cdot 10^{15}$				
$v = 10 \text{ km s}^{-1}$, $n(\text{H}_2) = 10^6 \text{ cm}^{-3}$						
WIND REGION (iii)						
T=100 K, $\theta = 10''$	$1.5 \cdot 10^{17}$	$5 \cdot 10^{15}$				
$v = 15 \text{ km s}^{-1}$, $n(\text{H}_2) = 3 \cdot 10^5 \text{ cm}^{-3}$						
T=50 K, $\theta = 20''$	$1.7 \cdot 10^{17}$	$5.7 \cdot 10^{15}$				
$v = 15 \text{ km s}^{-1}$, $n(\text{H}_2) = 10^4 \text{ cm}^{-3}$						

TABLE 7

Observed and predicted intensities for the mm and submm CO lines for each source.

Source		CO lines					
		1-0	2-1	3-2	4-3	6-5	7-6
CRL 2688	$I_{obs}(\text{Jy})$	30	70	271	373	640	760
	$I_{mod}(\text{Jy})$	10	30	296	429	650	790
CRL 618	$I_{obs}(\text{Jy})$	23	47	79		320	232
	$I_{mod}(\text{Jy})$	21	66	197	400	742	994
NGC7027	$I_{obs}(\text{Jy})$	36	70	364	516	520	840
	$I_{mod}(\text{Jy})$	24	83	475	498	893	1061

TABLE 8

Table of the molecular, atomic and ionic abundances (relative to ^{12}CO) in CRL 2688, CRL 618 and NGC 7027 as seen by the model.

Species	CRL 2688	CRL 618	NGC7027
^{13}CO	$< 1/25$	$1/20$	$\lesssim 1/30$
HCN	$< 1/30 - 1/100$	$1/10 - 1/1000$	
HNC		$1/10 - 1/1000$	
H ₂ O		$1/25$	$< 1/650$
OH		$1/1250$	$1/20$
[OI]		4.5	875
CH ⁺			$1/80$